A Virtual-Impedance Droop Control for Accurate Active Power Control and Reactive Power Sharing Using Capacitive-Coupling Inverters

Deng, Wenyang; Dai, Ning Yi; Lao, Keng Weng; Guerrero, Josep M.

Published in:
IEEE Transactions on Industry Applications

DOI (link to publication from Publisher):
10.1109/TIA.2020.3012934

Publication date:
2020

Document Version
Accepted author manuscript, peer reviewed version

A Virtual-Impedance Droop Control for Accurate Active Power Control and Reactive Power Sharing Using Capacitive-Coupling Inverters

Wenyang Deng, Ning Yi Dai, *Senior Member*, *IEEE*, Keng-Weng Lao, *Member, IEEE*, and Josep M. Guerrero, *Fellow, IEEE*

***Abstract*—Capacitive-coupling inverters (CCIs) have low operation voltage and enhanced reactive power control capability. It is a promising alternative to provide reactive power and voltage regulation in microgrids (MGs). Droop control is one of the most widely used primary controllers under a hierarchical framework in a MG. However, conventional droop control performance needs improvement since the droop curve assumption is not valid in part of CCI's operational area. At the same time, reactive power sharing error due to the uncertainty factor of feeder impedance needs to be minimized. In this paper, virtual-impedance droop control is proposed for CCIs to solve the two issues. A virtual impedance selection method is developed with consideration of CCI's second-order LC coupling branch. First, the virtual impedance is selected for reducing the coupling between the active and reactive power of CCIs. The stability and sensitivity of the system are also evaluated based on a small-signal model to provide guidelines for virtual impedance selection. The proposed control varies the equivalent impedance via a feed-back loop in CCI's control for accurate power control and sharing in MGs under mismatched feeder impedance. The validity of the proposed virtual-impedance droop control is verified through simulation and experimental results.**

***Index Terms*—Active power, Capacitive-coupling inverter, Microgrid, Reactive power, Virtual-impedance**

I. Introduction

A microgrid (MG) is small to medium-scale power system, usually formed by connecting distributed generation (DG) units and local load. It can operate in either grid-connected mode or islanded mode [1-3]. MGs can minimize the burden on transmission networks by supplying local loads and integrating distributed generation (DG) units [4-6]. One typical configuration of an MG is shown in Fig. 1.

Inverters play an important role in MGs, and multi-inverter control is a key part of a MG's control scheme [7]. Hierarchical control was proposed for maintaining power balance and coordinating all DG units in a MG [8-11]. The hierarchy usually includes primary, secondary, and tertiary layers, among which the primary control layer regulates DG units directly and generates the local control signal for inverters. Much effort has been put to develop local controllers for inverters in MGs. Droop-control is widely implemented in the power-control loop of a DG. It can achieve adaptive power regulation and automatic power sharing without any communication [12]. Conventional *P-f* and *Q-V* droops can easily achieve active power sharing. However, it has poor performance in reactive power sharing due to the effects of mismatched feeder impedance [13]-[16]. Virtual-impedance method has been developed to improve conventional droop-control [17-19]. This method was proved to be a valid solution for achieving accurate reactive power sharing under unknown feeder impedance situation [7].

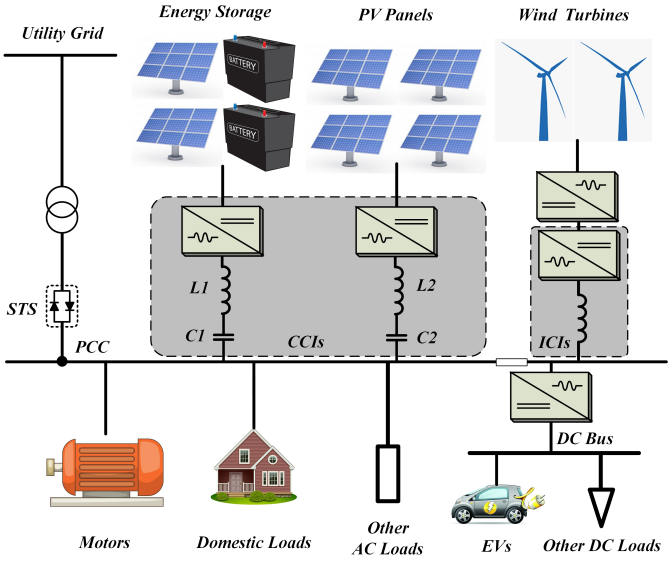

Fig. 1. Configuration of a microgrid.

This work was supported by the Sichuan Science Technology Program (2019JDPT0029) and University of Macau under the projects of MYRG2018-00097-FST and MYRG2019-00111-FST.

Wenyang Deng and Keng-Weng Lao are with the State Key Laboratory of Internet of Things for Smart City and Department of Electrical and Computer Engineering, University of Macau, Macao, People's Republic of China (e-mail: yb47446@um.edu.mo and johnnylao@um.edu.mo).

Ning Yi Dai is with the State Key Laboratory of Internet of Things for Smart City and Department of Electrical and Computer Engineering, University of Macau, Macao, and Zhuhai UM Science & Technology Research Institute, Zhuhai, People's Republic of China (e-mail: nydai@um.edu.mo).

J. M. Guerrero, is with the Department of Energy Technology, Aalborg University, 9220 Aalborg Ø, Denmark (e-mail: joz@et.aau.dk)

Various virtual-impedance droop control schemes were investigated. Accurate active and reactive power sharing can be achieved [20][21]. Some have the capability to enhance harmonic sharing [22][23]. Stability and transient response of the droop-controlled DG are focused on in [24][25]. Virtual-impedance droop control was investigated for MG in islanded mode [26] and a multi-bus MG [27].

However, it is noteworthy that all control methods, as mentioned above, are developed for inverters that are coupled to MG via inductor, LC filter, or LCL filters. They are named as the inductive-coupling inverter (ICI) since coupling impedance equals to one inductor in a fundamental frequency equivalent circuit. Reactive power compensation is usually an ancillary service provided by ICIs. The available capacity is hard to estimate. Instead, the separated unit may be used to provide reactive power in a MG, especially when it operates in islanded mode.

There is a trend to implement MGs with an increasing number of sources and loads. The intermittent output power of a renewable generation causes voltage deviation in MGs. In order to improve the efficiency and voltage stability of MGs, enhancing reactive power regulation capability is necessary [28][29]. Some inverters may take a leading role in reactive power control to meet the diversified regulation requirements. Capacitive-coupling inverter (CCI) was first proposed in the 1990s and named as hybrid power filter at that time [30]. Its modeling, design, and control has been extensively studied since then [31]-[34]. CCI was proved to be a low-cost solution for reactive power and harmonics in medium- and low-voltage applications.

It was named as CCI when it was used to integrate distributed generator (DG) units in a MG [29]. Hence, it can be distinguished from conventional inductive-coupling inverters. Capacitive-coupling inverter (CCI) is a promising solution for reactive power regulation in MGs [35 -36]. Its second-order series LC circuit increases the difficulty of developing its control method from existing solutions. For example, second-order non-linear current controller is studied in [34][37][38] and PR controller is studied in [35][39]. Droop-control method is also applied to control CCIs [28][36][40]. However, only control methods for single CCI was studied. Power sharing of CCIs in the MG was not investigated yet.

A comparison between ICI and CCI was provided [35]. Theoretically, a pre-set power control range can be fulfilled by both ICI and CCI if there is no limitation to the inverter's dc-link voltage. The previous analyses indicate that CCI takes advantage of its coupling impedance and provides an enhanced capability to regulate reactive power. At the same time, CCI is able to keep its dc voltage much lower than the grid-side voltage [35][36]. This low operation voltage results in reduced initial cost and switching losses and makes CCI more competitive in reactive power regulation for low and medium voltage applications.

In this paper, control of CCIs in a MG is investigated for accurate active power injection and reactive power sharing. CCI has a coupling impedance much higher than that of the ICI. Its coupled to the power grid via a second-order LC branch, which is modeled as a capacitor in a fundamental frequency equivalent circuit. Valid area of conventional *P-f* and *Q-V* droops will be analyzed, and virtual-impedance method for improving CCI's droop will be studied. Power sharing for CCIs was not investigated to the best of our knowledge. The main contributions of this paper include:

- Investigation valid operational area of conventional droop control for CCIs;
- Develop a virtual-impedance droop control for CCIs to achieve accurate active power injection and reactive power sharing in MG;
- Investigation of virtual-impedance selection for CCIs, which can reduce coupling between active and reactive power without affecting the transient response and stability margin.

This paper is organized as follows. The operational principle of CCIs and limitations of conventional droop control is introduced in Section II. Droop control with virtual impedance is proposed in Section III. In this Section, stability margin and transient response are also evaluated based on the small-signal model for further investigating virtual impedance selection. Simulation verifications are provided in Sections IV, and experimental results are given in Section V. Finally, a conclusion is presented in Section VI.

II. DROOP-CONTROLLED CCI

A. Operational principle of CCI

The application of droop control in CCIs and its limitations are first presented in this Section. Two parallel-connected CCIs are used for DG integration in Fig. 1. The inverter is coupled to the point of common coupling (PCC) via a second-order LC branch, which is designed according to reactive power control range and LC resonant frequency [29]. The fundamental frequency impedance of the LC coupling branch is expressed as follows.

$$Z_C = \frac{1}{\omega C} - \omega L \qquad \theta_C = -\frac{\pi}{2} \tag{1}$$

The active and reactive power injected by the parallel-connected inverter can then be expressed as:

$$P = \left(\frac{VE}{Z}\cos\delta - \frac{E^2}{Z}\right)\cos\theta + \frac{VE}{Z}\sin\delta\sin\theta \tag{2}$$

$$Q = \left(\frac{VE}{Z}\cos\delta - \frac{E^2}{Z}\right)\sin\theta - \frac{VE}{Z}\sin\delta\cos\theta \tag{3}$$

,where the symbols are defined as follows:
E: RMS amplitude of grid-side voltage
V: RMS voltage of inverter output voltage
Z: Impedance of coupled structure
θ: Phase angle of coupled impedance
δ: Phase angle between V and E

Since CCI is coupled to the system via coupling impedance given in (1), (4) is obtained.

$$P^2+\left(Q-\frac{E^2}{Z_C}\right)^2=\left(\frac{VE}{Z_C}\right)^2 \tag{4}$$

Power control range of a CCI is shown in Fig. 2, which is obtained by assuming that $S_{base}=E^2/Z_C$. The vertical axis depicts the ratio of CCI's output voltage to grid-side voltage. As illustrated in Fig. 2, CCI is able to operate with its output voltage lower than grid-side voltage within a certain range. This characteristic makes CCI a supplementary solution for power conditioning in a MG.

B. *Droop control for CCI and its valid operational area*

Conventional *P-f* and *Q-V* droops regulate frequency or phase angle of the inverter output voltage by active power, while output voltage amplitude changes according to reactive power. Therefore, decoupling control of active and reactive power is achieved. The following droop controller has been widely used as the primary control for parallel-connected ICIs in MGs. It will be used to control CCI in this paper too.

$$\omega=\omega^*-m\left(P-P_{ref}\right) \tag{5}$$

$$V=E-\left(k_p+\frac{k_i}{s}\right)\left(Q-Q_{ref}\right) \tag{6}$$

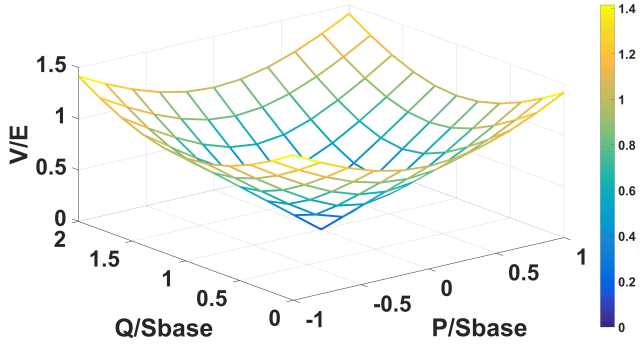

Fig.2. Power control range of a CCI

According to (5) and (6), decoupling control of active power and reactive power can be implemented. However, the basic droop control algorithm is obtained based on the assumption that δ in (2) and (3) is in the vicinity of zero. As a result, the valid operational area of droop control can be evaluated by considering phase angle variation. Basically, power control error increases as δ increase and can be estimated by:

$$Error=\left|\frac{\delta-\sin\delta}{\sin\delta}\right|*100\% \tag{7}$$

The relationship between error and phase angle is illustrated in Fig. 3. If a threshold of 2% is set for error in (7), the corresponding value of δ_{max} is about 0.35π. When the range of phase angle is limited to [$-\delta_{max}$, δ_{max}], decoupling control of active and reactive power is only valid within two shaded sectors in Fig. 3. Hence, errors will be introduced by droop control if CCI operates outside these two sectors.

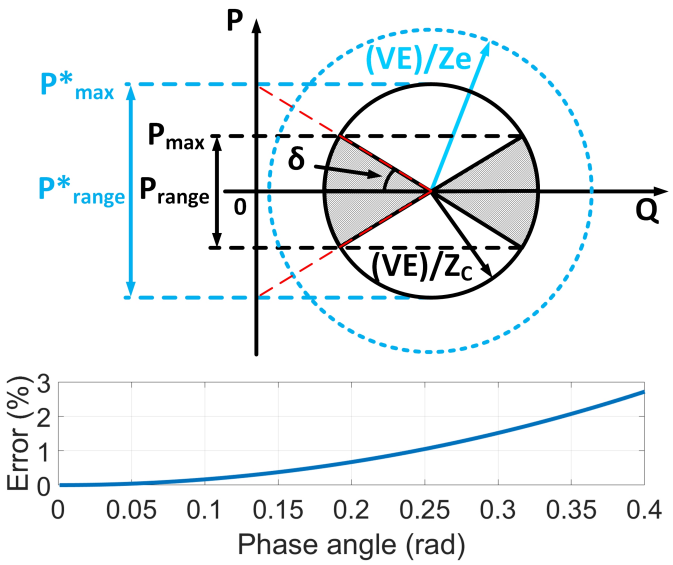

Fig. 3. Error analyses of droop control for CCIs

However, the theoretical power control range of a CCI is bounded by a circle based on (4) and radius of the circle is inversely proportional to Z_C, which is the fundamental frequency impedance of CCI's coupling branch. A solid black circle is shown in Fig. 3 to indicate this boundary. The conventional droop control introduces power control error outside the two shaded sectors, which also affect the accuracy of power sharing. As a result, improved droop control is necessary for making full use of CCI's power control capability and will be investigated in the next Section.

III. Virtual-Impedance Droop Control

A. *Virtual-impedance droop control*

A virtual-impedance droop control is developed for CCIs in this paper. Instead of changing physical coupling impedance, virtual impedance feed-back loop is added to CCI's control system, and the control block diagram is shown in Fig. 4. After the virtual impedance loop is added, the equivalent coupling impedance is revised as:

$$Z_e e^{j\theta_e}=Z_C e^{j\theta_C}-Z_v e^{j\theta_v} \tag{8}$$

, where Z_C and θ_C are the amplitude and angle of physical coupling impedance, respectively; Z_v and θ_v are the amplitude and angle of virtual impedance, respectively.

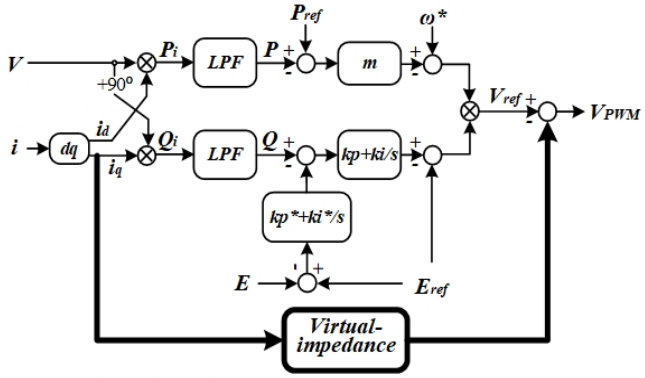

Fig.4. Virtual-impedance droop control for CCIs

B. Power control range extension

First, the proposed virtual-impedance method is able to reduce coupling impedance without using a bulky coupling capacitor. Previous analysis shows that the valid power decoupling range of conventional droop control is in the range of [$-\delta_{max}$, δ_{max}]. Hence, P_{max} in Fig.3 can be calculated as follow.

$$P_{max}=\left(\frac{VE}{Z_C}cos\,\delta_{max}-\frac{E^2}{Z_C}\right)cos\,\theta_C+\frac{VE}{Z_C}sin\,\delta_{max}\,sin\,\theta_C \quad (9)$$

Reducing coupling impedance can extend this range. However, to increase the coupling capacitance of CCI increases physical size and cost. The proposed virtual-impedance droop control changes equivalent impedance by virtual impedance. According to (8), maximum active power is changed to:

$$P_{max,v}=\left(\frac{VE}{Z_e}cos\,\delta_{max}-\frac{E^2}{Z_e}\right)cos\,\theta_e+\frac{VE}{Z_e}sin\,\delta_{max}\,sin\,\theta_e \quad (10)$$

The new maximum value should meet the following condition.

$$P_{max,v}\geq P_{max} \quad (11)$$

P_{max} is set concerning the required active power control range. Therefore, a boundary for selecting equivalent impedance is deduced by assuming $Z_e e^{j\theta_e}=R+jX$ and substituting it to (10).

$$P_{max}Z_e^2-VE\left(R\,cos\,\delta_{max}-X\,sin\,\delta_{max}\right)+RE^2\leq 0 \quad (12)$$

The coupling impedance boundary in (12) is shown in Fig. 5, in which boundaries are deduced for several P_{max}. Related parameters are given in Table I for plotting Fig. 5. The equivalent impedance of a CCI should be selected inside the boundary concerning the required active power control range.

TABLE I
MAIN PARAMETERS USED IN CASE STUDY

Parameter	Value
δ_{max}	0.35rad
E	110V
V/E	0.9
K_{Re}	-7
$K_{Im\text{-}min}$	0.55
$K_{Im\text{-}max}$	1.4

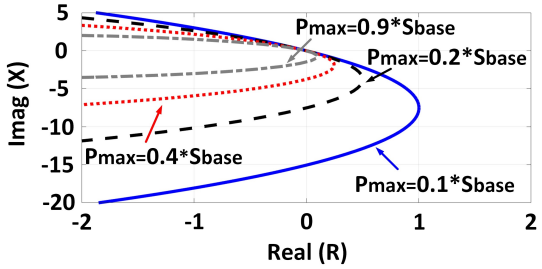

Fig.5. Equivalent impedance boundaries with respect to the maximum active power of a CCI

C. Stability Margin and Transient Response Analyses for proposed virtual-impedance droop control

Since an extra feed-back loop is added to CCI's control system by the proposed virtual-impedance method, stability and transient response need to be evaluated for virtual-impedance selection. A small-signal model is deduced. It is assumed that the grid-side voltage is Ee^{j*0}, CCI's output voltage is $Ve^{j*\delta}$, and the coupling impedance is $Ze^{j*\theta_e}$. The apparent power injecting to the grid by a CCI is expressed as:

$$\vec{S}=\vec{V}*\vec{I}=\frac{V^2}{Z_e}*e^{-j*\theta_e}-\frac{VE}{Z_e}*e^{-j*(\delta-\theta_e)} \quad (13)$$

When there is a small disturbance at the equilibrium point, small-signal equations of a CCI are as follows.

$$\begin{aligned}\Delta\omega&=-m*\Delta P\\ \Delta V&=-\left(k_p+\frac{k_i}{s}\right)*\Delta Q\end{aligned} \quad (14)$$

With disturbances in (14), the small-signal power variations are obtained.

$$\begin{aligned}\Delta P&=-\frac{1}{\tau s+1}\Delta P'\\ \Delta Q&=-\frac{1}{\tau s+1}\Delta Q'\end{aligned} \quad (15)$$

$$\begin{aligned}\Delta P'&=Re\left(\frac{\partial\vec{S}}{\partial\delta}\right)*\Delta\delta+Re\left(\frac{\partial\vec{S}}{\partial V}\right)*\Delta V\\ \Delta Q'&=Im\left(\frac{\partial\vec{S}}{\partial\delta}\right)*\Delta\delta+Im\left(\frac{\partial\vec{S}}{\partial V}\right)*\Delta V\end{aligned} \quad (16)$$

Since $\Delta\omega=s*\Delta\delta$, the small-signal model is established as:

$$\left[A(s)-B(s)*C(s)\right]*K=0 \quad (17)$$

, where definitions are as follows:

$$K=\begin{bmatrix}\Delta\delta\\ \Delta V\end{bmatrix};$$

$$A(s)=\begin{bmatrix}s(\tau s+1) & 0\\ 0 & s(\tau s+1)\end{bmatrix};$$

$$B(s)=\begin{bmatrix}-m & 0\\ 0 & -(s*k_p+k_i)\end{bmatrix};$$

$$C(s)=\begin{bmatrix}Re\left(\frac{\partial\vec{S}}{\partial V}\right) & Re\left(\frac{\partial\vec{S}}{\partial\delta}\right)\\ Im\left(\frac{\partial\vec{S}}{\partial V}\right) & Im\left(\frac{\partial\vec{S}}{\partial\delta}\right)\end{bmatrix}$$

After virtual impedance is applied to CCI's control system, the equivalent impedance of a CCI is changed. However, proper stability and transient performance should be maintained. Hence, the equivalent impedance needs to meet the following constraints.

- Since system damping is mainly affected by the imaginary conjugate poles, damping ratio needs to satisfy the following constraint:

$$K_{Im-min} \le \left| \frac{Im_{(poles)}}{Re_{(poles)}} \right| \le K_{Im-max} \tag{18}$$

- The real part of all poles should be less than K_{Re} to guarantee enough stability margin:

$$Max(Re_{(poles)}) \le K_{Re} \tag{19}$$

Root locus is shown in Fig.6 (a). According to Routh-Hurwitz stability criterion, if all roots are located on the left of the imaginary axis, the system is stable. Impedance boundaries are obtained and shown in Fig.6 (b) by setting different stability margin and damping ratio. It can be found in Fig. 6 that coupling impedance cannot be set too small in order to reserve enough stability margin. Also, the two conjugate poles approach the real axis as coupling impedance increases.

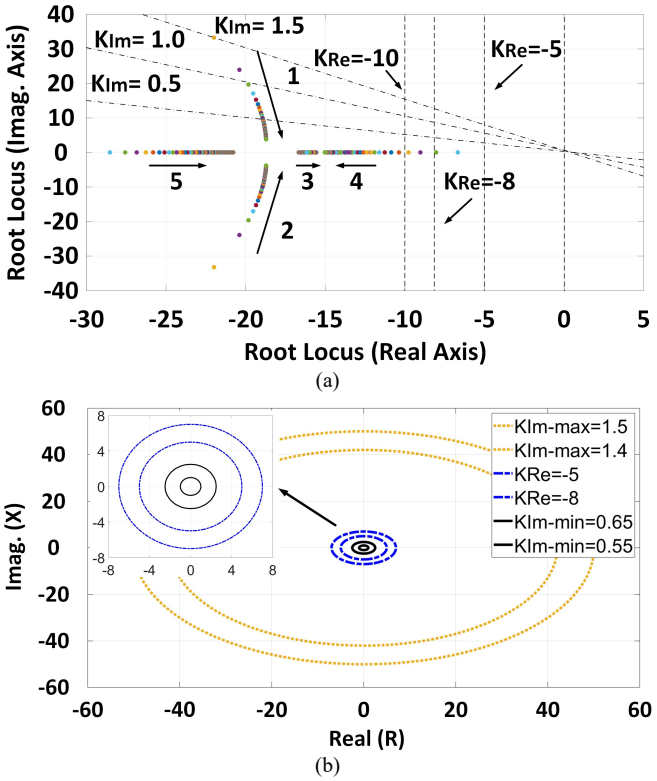

Fig.6. Equivalent impedance range obtained from small-signal model analysis (a) Root Locus (b) Impedance range

D. Virtual-Impedance Selection

The key point of the proposed virtual-impedance droop control is virtual-impedance selection. According to (8), virtual impedance can be calculated by using the following formula.

$$Z_v e^{j\theta_v} = Z_C e^{j\theta_C} - Z_e e^{j\theta_e} \tag{20}$$

The coupling impedance $Z_C e^{j\theta_C}$ is the physical impedance of a CCI. The equivalent impedance $Z_e e^{j\theta_e}$ needs to be selected by considering the power control range extension, stability margin, and transient performance. In summary, the parameters in Table I is used as a case study, and virtual impedance design steps are listed below.

- Step 1: According to (12), a boundary for selecting coupling impedance is deduced for a target P_{max}. Since the coupling resistor is usually kept as low as possible, it is assumed that coupling resistor is limited to a small range near $R=0$. Therefore, only the shaded part in graph 1 of Fig.7 will be further considered for coupling impedance selection.
- Step 2: Based on the condition in (18), two boundaries of coupling impedance are deduced. The inner boundary is a circle centered at (0, 0) with a radius of 1.6. The outer boundary is a circle centered at (0, 0) as well, but with a radius of 40. For a better view, only the inner boundary is shown in Fig. 7. As a result, the region for coupling impedance selection is reduced to the shaded part in graph 2 of Fig.7.
- Step 3: Based on the condition in (19) and stability margin parameter K_{Re} in Table I, a boundary of coupling impedance is deduced, which is a circle centered at (0, 0) with the radius of 2.5. The region for coupling impedance selection is reduced to the shaded part in graph 3 of Fig.7.
- Step 4: The equivalent impedance is selected from the intersection area of the results obtained from the previous three steps. Low impedance is preferred, so that equivalent impedance is usually selected, close to the upper boundary of the region in graph 4 of Fig.7. It is then substituted to (20), and the virtual impedance is obtained.

The frequency response of the coupling impedance without and with virtual impedance is shown in Fig. 8. The obtained virtual impedance is used in the proposed control and will be verified hereinafter.

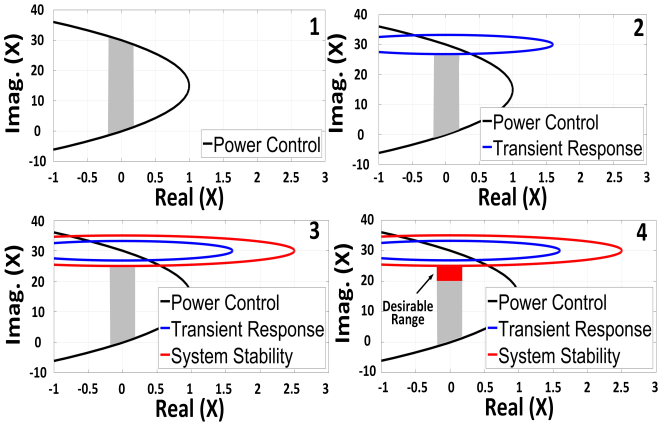

Fig. 7. Design example of equivalent impedance

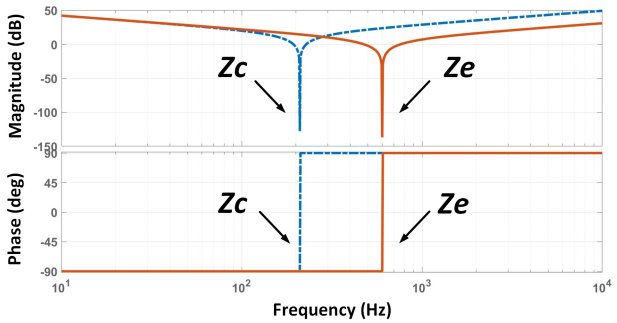

Fig.8. Coupling impedance (Z_c) and equivalent impedance (Z_e)

IV. Simulation Verification

In order to verify the effectiveness of the proposed virtual-impedance droop control for CCIs, a simulation model is built by using Matlab/Simulink.

A. Virtual-impedance droop control for accurate power control

Single CCI is tested first by applying the control block diagram in Fig. 4. The system configuration is shown in Fig.9, and related parameters are given in Table II. To better illustrate the power tracking error, active and reactive power references are pre-set in the control system in this part. The accurate power control range of conventional droop control is the dashed sectors in Fig.3. However, the theoretical power control boundary of a CCI is bounded by a circle. In order to illustrate the effectiveness of the proposed control method, five testing points are selected, as shown in Fig.10. Points A locates inside the accurate power control region of droop control. Points B, C, D, and E are all outside the accurate power control region.

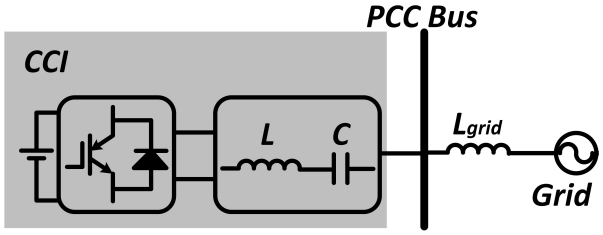

Fig.9. Circuit configuration of parallel-connected CCIs

TABLE II
Parameters of The Simulation Model

Parameter	Value
DC-link voltage V_{DC}	80 V
PCC voltage E	110 V
Coupling Inductance L	3.8 mH
Coupling Capacitance C	121 μF
Virtual-impedance $X_{virtual}$	$6\pi e^{j90}$

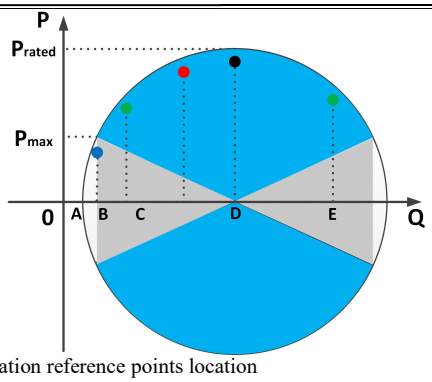

Fig.10. Simulation reference points location

Power references for CCI are calculated according to the location of points A to E. Droop control without virtual impedance is used to control a CCI first. Then CCI is controlled by virtual-impedance droop control. Simulation results are summarized in Table III for all five cases. It is evident that better power control accuracy is achieved when virtual-impedance loop is added to droop control. In particular, active power tracking error is high for droop control when testing points locate outside two dashed sectors. The proposed method effectively reduces the power tracking error. For example, active power tracking error is reduced from 14% to 0.5% at testing point C. The reactive power control is improved accordingly since virtual impedance affects both phase angle and amplitude of inverter's output voltage.

Active and reactive power variations of CCI are shown in Fig. 11 and Fig. 12, respectively. In each figure, the upper one is obtained by using droop control, and the lower one is obtained by virtual-impedance droop control. The operation points of CCI changes from one to another in each figure. The dynamic performance of the CCI is verified too.

TABLE III
Simulation Results of Power Control of Single CCI

No.	Power Ref.		Without Virtual Impedance		With Virtual Impedance	
			Value	Error	Value	Error
A	P	40	37	7.5%	41	2.5%
	Q	300	304	1.3%	299	0.3%
B	P	70	66	5.7%	71	1.4%
	Q	400	405	1.3%	402	0.5%
C	P	200	172	14.0%	201	0.5%
	Q	460	470	2.1%	458	0.4%
D	P	120	112	6.7%	122	1.6%
	Q	540	527	2.4%	538	0.4%
E	P	50	47	6.0%	49	2%
	Q	700	691	1.3%	703	0.4%

B. Virtual-impedance droop control for parallel-connected CCIs

In this part, parallel-connected CCIs are controlled by the proposed virtual-impedance droop control. The system configuration is shown in Fig.13. The impact of impedance mismatch will be studied. Parameters of parallel-connected CCIs are given in Table IV. Errors are introduced in coupling capacitance and feeder inductance. In the simulation, both two CCIs provide reactive power for regulating the voltage at the PCC. Hence, the reactive power reference of each CCI is obtained from a voltage regulation loop, as shown in Fig. 4. The proposed virtual-impedance droop control is used to control the active power and reactive power of each CCI.

The active and reactive power variations are recorded and shown in Fig.14 and Fig. 15, respectively. In each figure, the upper one is obtained by using droop control, and the lower one is obtained by using the proposed method. It is obvious that the proposed method not only improves the power tracking accuracy of each CCI; it also increases power sharing accuracy at the same time without being affected by impedance mismatch. In addition, the voltage at the PCC is shown in Fig. 16. The CCIs could regulate reactive power to compensate voltage drop when loads are suddenly increased in a MG.

This article has been accepted for publication in a future issue of this journal, but has not been fully edited. Content may change prior to final publication. Citation information: DOI 10.1109/TIA.2020.3012934, IEEE Transactions on Industry Applications

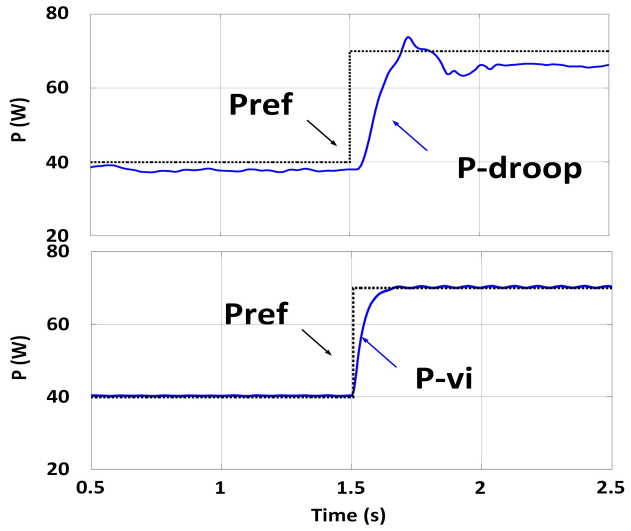

(a) Active power from points A to B

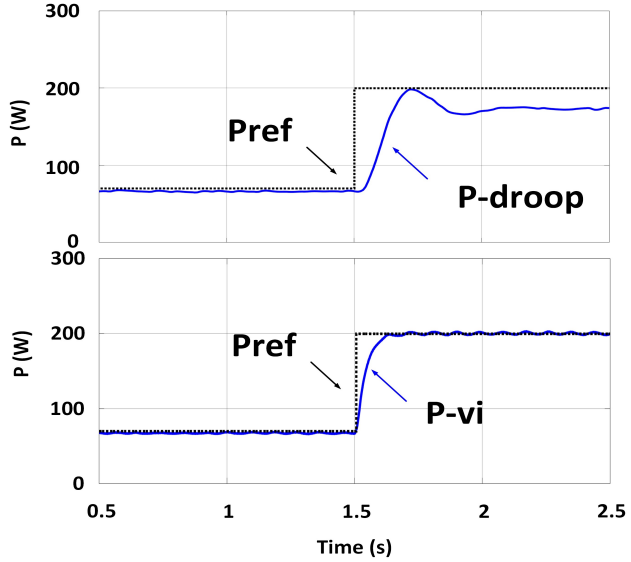

(b) Active power from points B to C

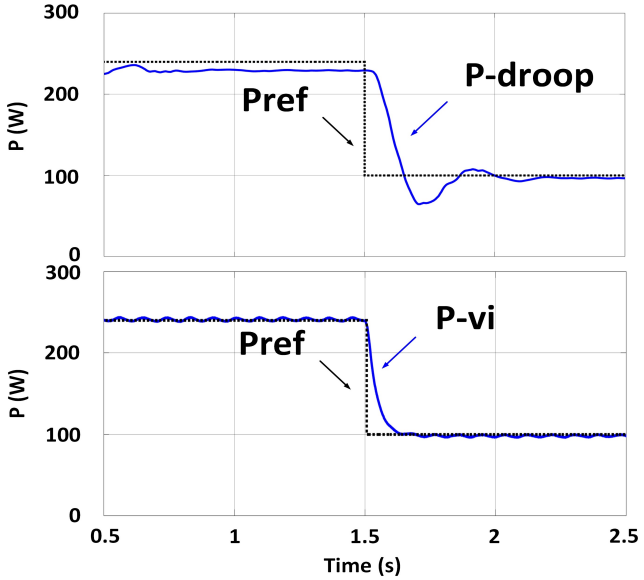

(c) Active power from points D to E

Fig.11. Comparison of active power variation with and without virtual-impedance control loop

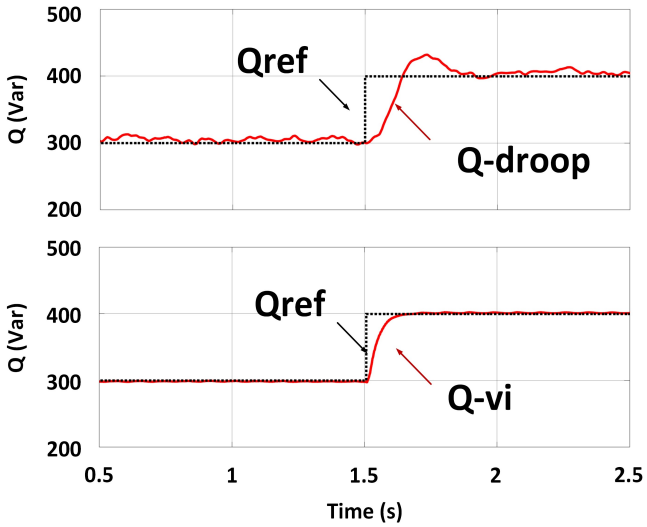

(a) Reactive power from points A to B

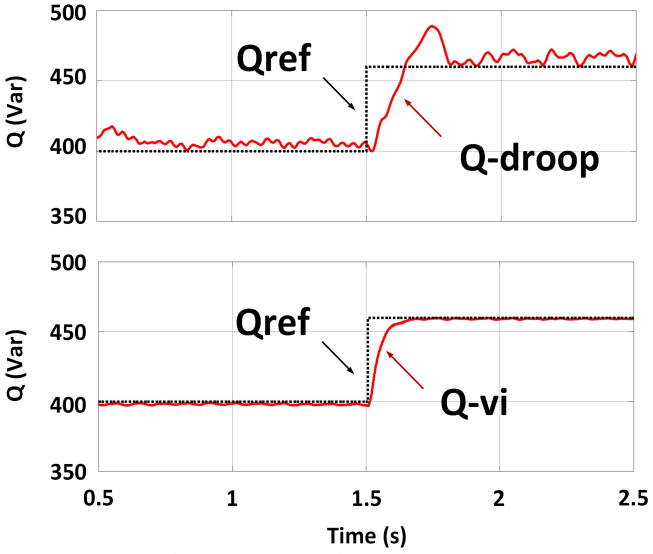

(b) Reactive power from points B to C

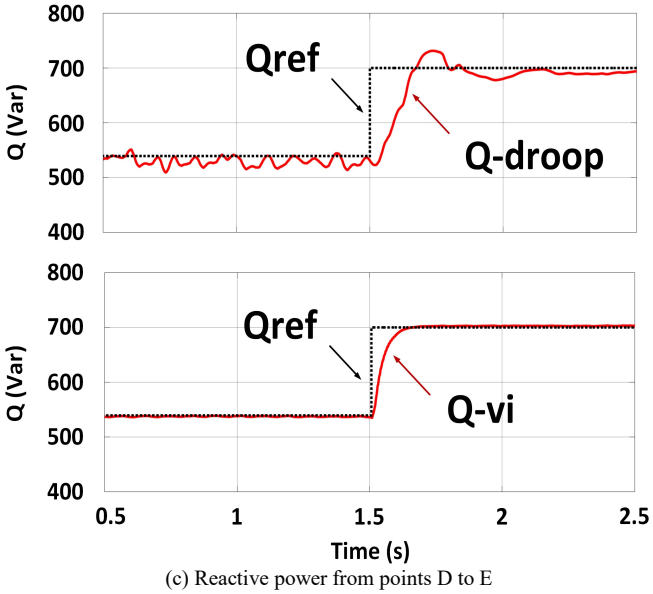

(c) Reactive power from points D to E

Fig.12. Comparison of reactive power variation with and without virtual-impedance control loop

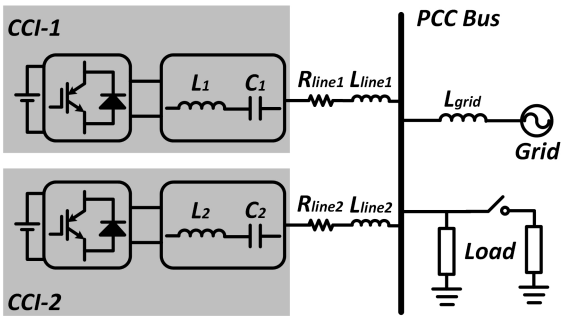

Fig.13. Circuit configuration of parallel-connected CCIs

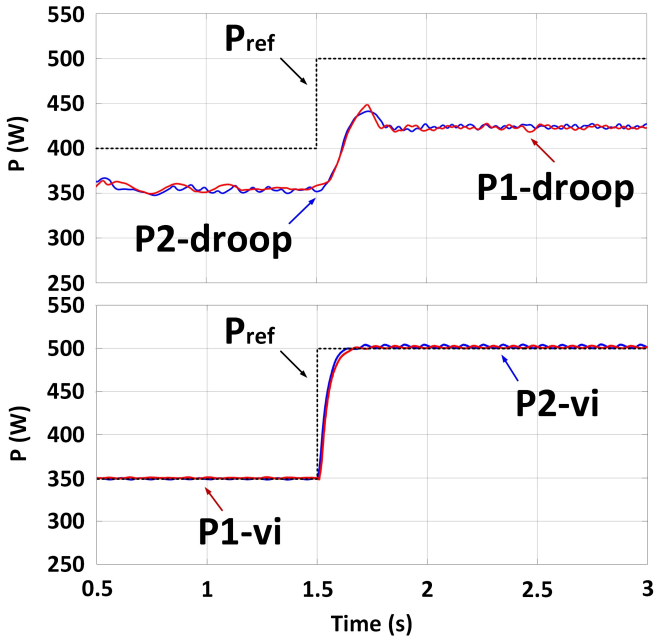

Fig.14. Comparison of active power variation of parallel-connected CCIs with and without virtual-impedance control loop

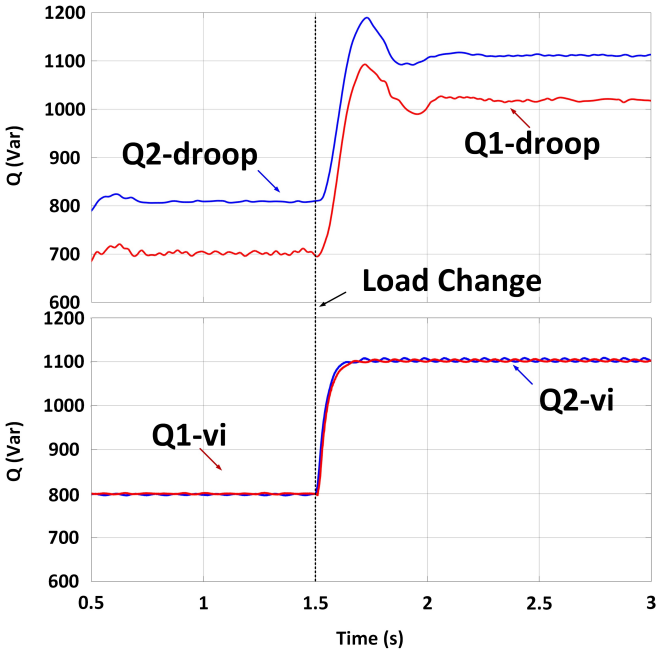

Fig.15. Comparison of reactive power variation of parallel-connected CCIs with and without virtual-impedance control loop

TABLE IV
PARAMETERS OF PARALLEL-CONNECTED CCIS

Parameter	Value	
	CCI 1	CCI 2
DC-link voltage V_{DC}	110 V	
PCC voltage E	110 V	
Coupling Inductance	3.8mH	
Coupling Capacitance	280μF	300μF
Feeder Resistance	0.1Ω	0.15Ω
Feeder Inductance	0.5mH	0.75mH
Virtual-impedance $X_{virtual}$	πe^{j90}	

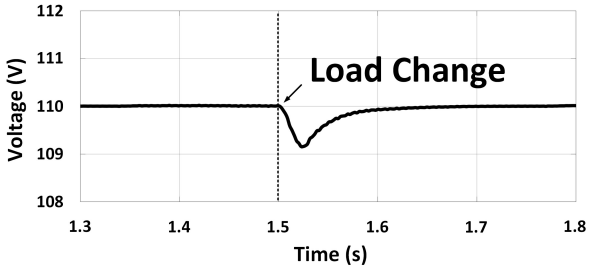

Fig.16. PCC voltage variation under load change

V. EXPERIMENTAL RESULTS

The lab-scale prototype of parallel-connected CCIs is shown in Fig. 17. The testing system configuration is the same as that used in the simulation. The control algorithm is implemented by an RT-unit digital controller.

A. Virtual-impedance droop control for single CCI

In this part, detailed system parameters are almost the same as those in Table II. In order to verify the validity of the proposed control method in improving power control accuracy, five testing points are selected, similar to those used in the simulation. Experimental results are shown in Fig. 18, which are recorded for cases A to E. Power, voltage, and currents recorded from CCI-side, source-side, and load-side are recorded. The experiment results are summarized in Table V.

Results indicate that power control accuracy is improved by using virtual-impedance droop control. For example, there is an apparent error reduction from 17% to 0.5% in Case C. In summary, CCI reduces active power consumption at the source side by injecting active power to PCC. It also improves the power factor at the source side by injecting reactive power. The source side power factor is all approaching unity in the experimental results since reactive power reference is deduced from calculating reactive load power in the experiment in this part.

TABLE V
EXPERIMENTAL RESULTS

No.		Power Ref.	Without Virtual Impedance		With Virtual Impedance	
			Value	Error	Value	Error
A	P	40	38	5%	39	2.5%
	Q	300	304	1.3%	301	0.3%
B	P	70	63	9%	72	2.8%
	Q	400	390	2.5%	395	1.3%
C	P	200	165	17%	201	0.5%
	Q	460	470	2%	468	1.7%
D	P	120	109	9%	120	0
	Q	540	525	2.4%	550	1.8%
E	P	50	47	6%	50	0
	Q	700	687	1.8%	690	1.4%

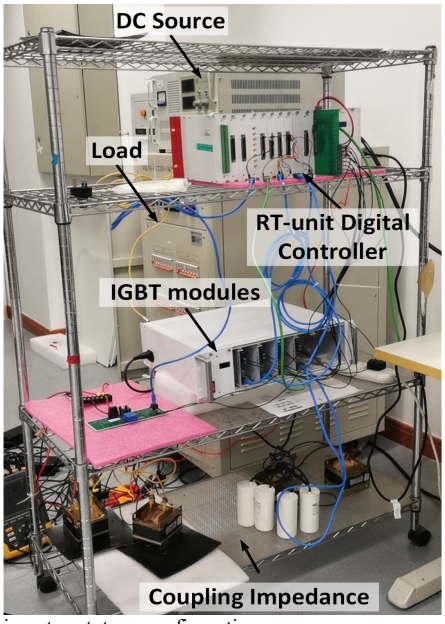

Fig.17. Experiment prototype configuration

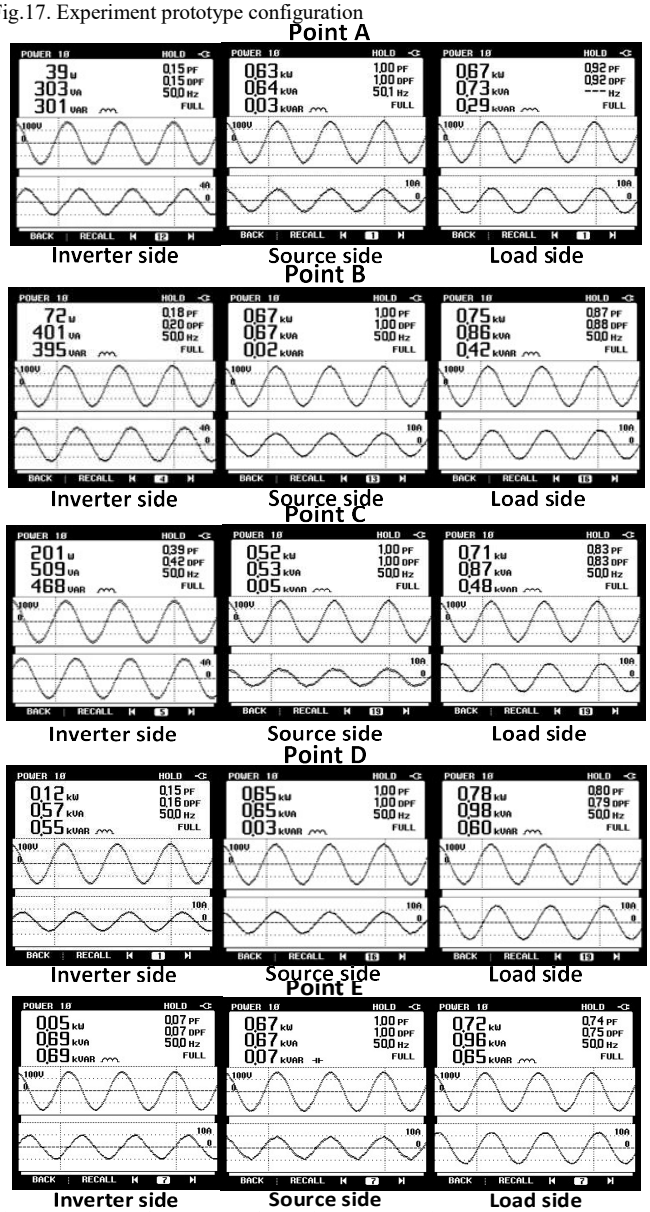

Fig.18. Power analyzer screenshots of every test point

B. Virtual-impedance droop control for paralleled-connected CCIs

In this part, parallel-connected CCIs in Fig.13 is controlled by the proposed virtual-impedance droop control. Detailed system parameters are listed in Table IV. The reactive power reference of each CCI is deduced by the voltage regulation controller. Active and reactive power of each CCI are recorded. Both droop control and virtual-impedance droop control are used to control parallel-connected CCIs. Experimental results are provided in Figs. 19 and 20, respectively.

Results indicate that the proposed virtual- impedance droop control make CCI track active power reference accurately. Reactive power sharing between two CCIs is also implemented by the proposed control; even errors exist in CCIs' coupling impedance. In addition, PCC voltage variation is shown in Fig. 21 to verify CCIs' capability in voltage regulation after a sudden load change.

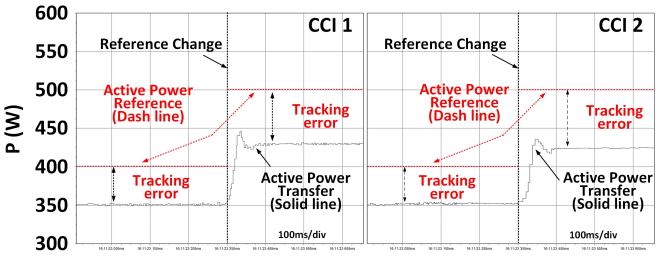

(a) Active power

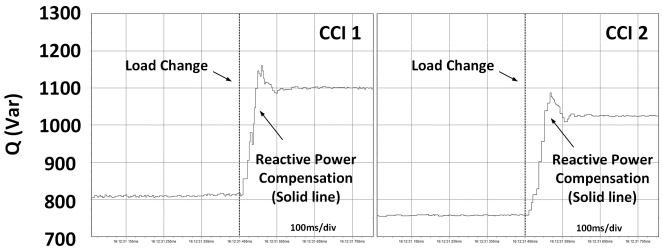

(b) Reactive power

Fig.19. Active and reactive power variation by using droop control

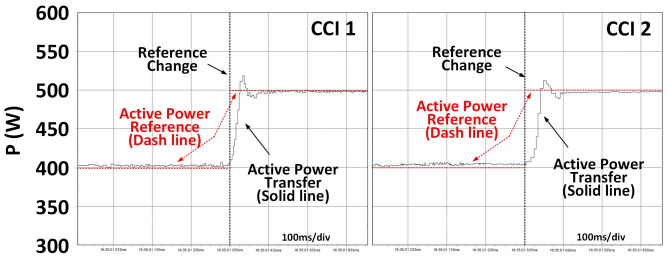

(a) Active power

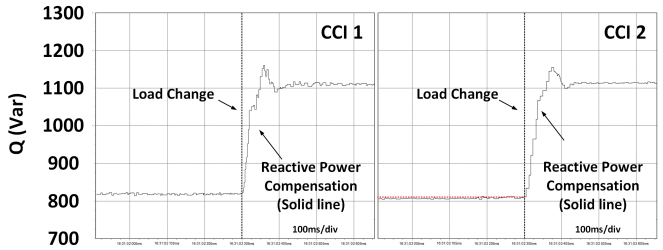

(b) Reactive power

Fig. 20. Active and reactive power variation by using proposed virtual-impedance droop control

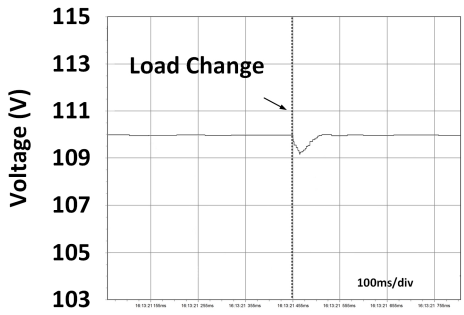

Fig.21. Experimental waveforms of voltage at PCC

VI. CONCLUSION

In this paper, virtual-impedance droop control is proposed for CCIs in a MG. It is noteworthy that CCI's power control characteristic is different from conventional inductive-coupling inverters. Therefore, it is a promising solution to enhance reactive power control capability in MGs, especially for voltage regulation. However, conventional droop control applied to CCI needs improvement. Otherwise, it results in unaccepted errors within the theoretical power control range of CCI. In order to tackle this problem, a virtual impedance loop and its selection method are proposed for CCI. With the proposed virtual impedance design technique, the power control accuracy of CCI is greatly enhanced, and reactive power sharing is improved too. It can thus contribute to the more effective application of CCI in the power grid. The proposed control technique is verified by means of simulation and experimental results. The proposed control method can be used as the primary control for CCIs in a hierarchical controlled MG with both CCI and ICI.

REFERENCES

[1] M. Pulcherio, M. S. Illindala, J. Choi and R. K. Yedavalli, "Robust Microgrid Clustering in a Distribution System with Inverter-Based DERs," in *IEEE Trans. Ind. Appl.*, vol. 54, no. 5, pp. 5152-5162, Sept.-Oct. 2018.

[2] Micallef, M. Apap, C. Spiteri-Staines and J. M. Guerrero, "Mitigation of Harmonics in Grid-Connected and Islanded Microgrids Via Virtual Admittances and Impedances," in *IEEE Trans. Smart Grid*, vol. 8, no. 2, pp. 651-661, March 2017.

[3] M. H. J. Bollen et al., "Power Quality Concerns in Implementing Smart Distribution-Grid Applications," in *IEEE Trans. Smart Grid*, vol. 8, no. 1, pp. 391-399, Jan. 2017.

[4] Wei, J. M. Guerrero, J. C. Vásquez and X. Guo, "A Circulating-Current Suppression Method for Parallel-Connected Voltage-Source Inverters with Common DC and AC Buses," in *IEEE Trans. Ind. Appl.*, vol. 53, no. 4, pp. 3758-3769, July-Aug. 2017.

[5] H. R. Baghaee, M. Mirsalim, G. B. Gharehpetian and H. A. Talebi, "Three-phase AC/DC power-flow for balanced/unbalanced microgrids including wind/solar, droop-controlled and Electronically-coupled distributed energy resources using radial basis function neural networks," in *IET Power Electron.*, vol. 10, no. 3, pp. 313-328, Mar. 2017.

[6] M. Zhang et al., "Cooperative Operation of DG Inverters and a RIHAF for Power Quality Improvement in an Integrated Transformer-Structured Grid-Connected Microgrid," in *IEEE Trans. Ind. Appl.*, vol. 55, no. 2, pp. 1157-1170, March-April 2019.

[7] F. Delfino, G. Ferro, M. Robba and M. Rossi, "An Energy Management Platform for the Optimal Control of Active and Reactive Powers in Sustainable Microgrids," in *IEEE Trans. Ind. Appl.*, vol. 55, no. 6, pp. 7146-7156, Nov.-Dec. 2019.

[8] K. Mahmud, A. K. Sahoo, J. Ravishankar and Z. Y. Dong, "Coordinated Multilayer Control for Energy Management of Grid-Connected AC Microgrids," in *IEEE Trans. Ind. Appl.*, vol. 55, no. 6, pp. 7071-7081, Nov.-Dec. 2019.

[9] Y. Han, P. Shen, X. Zhao and J. M. Guerrero, "Control Strategies for Islanded Microgrid Using Enhanced Hierarchical Control Structure with Multiple Current-Loop Damping Schemes," in *IEEE Trans. Smart Grid*, vol. 8, no. 3, pp. 1139-1153, May 2017.

[10] Y. Xia, Y. Peng and W. Wei, "Triple droop control method for ac microgrids," in *IET Power Electron.*, vol. 10, no. 13, pp. 1705-1713, Oct. 2017.

[11] Z. Zhao, P. Yang, J. M. Guerrero, Z. Xu and T. C. Green, "Multiple-Time-Scales Hierarchical Frequency Stability Control Strategy of Medium-Voltage Isolated Microgrid," in *IEEE Trans. Power Electron.*, vol. 31, no. 8, pp. 5974-5991, Aug. 2016.

[12] Y. Zhang and Y. W. Li, "Energy Management Strategy for Supercapacitor in Droop-Controlled DC Microgrid Using Virtual Impedance," in *IEEE Trans. Power Electron.*, vol. 32, no. 4, pp. 2704-2716, April 2017.

[13] M. Kallamadi and V. Sarkar, "Enhanced real-time power balancing of an AC microgrid through transiently coupled droop control," in *IET Gener. Transm. Distrib.*, vol. 11, no. 8, pp. 1933-1942, Jul. 2017.

[14] P. Zhang, H. Zhao, H. Cai, J. Shi and X. He, "Power decoupling strategy based on 'virtual negative resistor' for inverters in low-voltage microgrids," in *IET Power Electron.*, vol. 9, no. 5, pp. 1037-1044, Apr. 2016.

[15] R. Han, L. Meng, G. Ferrari-Trecate, E. A. A. Coelho, J. C. Vasquez and J. M. Guerrero, "Containment and Consensus-Based Distributed Coordination Control to Achieve Bounded Voltage and Precise Reactive Power Sharing in Islanded AC Microgrids", in *IEEE Trans. Ind. Appl.*, vol. 53, no. 6, pp. 5187-5199, Nov.-Dec. 2017.

[16] X. Guo, W. Liu, and Z. Lu, ''Flexible power regulation and current-limited control of the grid-connected inverter under unbalanced grid voltage faults,'' *IEEE Trans. Ind. Electron*., vol. 64, no. 9, pp. 7425–7432, Sep. 2017.

[17] H. Xu, X. Zhang, F. Liu, R. Shi, C. Yu and R. Cao, "A Reactive Power Sharing Strategy of VSG Based on Virtual Capacitor Algorithm," *IEEE Trans. Ind. Electron..*, vol. 64, no. 9, pp. 7520-7531, Sept. 2017.

[18] Q. Zhong and Y. Zeng, "Control of Inverters Via a Virtual Capacitor to Achieve Capacitive Output Impedance," in *IEEE Trans. Power Electron.*, vol. 29, no. 10, pp. 5568-5578, Oct. 2014.

[19] K. Wang, X. Yuan, Y. Geng and X. Wu, "A Practical Structure and Control for Reactive Power Sharing in Microgrid," *IEEE Trans. Smart Grid*, vol. 10, no. 2, pp. 1880-1888, March 2019.

[20] L. Huang, H. Xin, Z. Wang, L. Zhang, K. Wu, and J. Hu, ''Transient stability analysis and control design of droop-controlled voltage source converters considering current limitation,'' *IEEE Trans. Smart Grid*, vol. 10, no. 1, pp. 578–591, Jan. 2019.

[21] Trivedi and M. Singh, ''L1 adaptive droop control for AC microgrid with small mesh network,'' *IEEE Trans. Ind. Electron.*, vol. 65, no. 6, pp. 4781–4789, Jun. 2018

[22] Y. Qi, P. Lin, Y. Wang and Y. Tang, "Two-Dimensional Impedance-Shaping Control With Enhanced Harmonic Power Sharing for Inverter-Based Microgrids," in *IEEE Trans. Power Electron.*, vol. 34, no. 11, pp. 11407-11418, Nov. 2019

[23] T. V. Hoang and H. Lee, "Accurate Power Sharing With Harmonic Power for Islanded Multibus Microgrids," in *IEEE J. Emerg. Sel. Topics Power Electron.*, vol. 7, no. 2, pp. 1286-1299, June 2019

[24] A. S. Vijay, D. K. Dheer, A. Tiwari and S. Doolla, "Performance Evaluation of Homogeneous and Heterogeneous Droop-Based Systems in Microgrid—Stability and Transient Response Perspective," in *IEEE Trans. Energy Convers.*, vol. 34, no. 1, pp. 36-46, March 2019

[25] D. K. Dheer, V. A.S., O. V. Kulkarni and S. Doolla, "Improvement of Stability Margin of Droop-Based Islanded Microgrids by Cascading of Lead Compensators," in *IEEE Trans. Ind. Appl.*, vol. 55, no. 3, pp. 3241-3251, May-June 2019

[26] R. Wai, Q. Zhang and Y. Wang, "A Novel Voltage Stabilization and Power Sharing Control Method Based on Virtual Complex Impedance for an Off-Grid Microgrid", in *IEEE Trans. Power Electron.*, vol. 34, no. 2, pp. 1863-1880, Feb. 2019

[27] R. Razi, H. Iman-Eini, M. Hamzeh and S. Bacha, "A novel Extended Impedance-Power droop for accurate active and reactive power sharing in a multi-bus microgrid with complex impedances," in *IEEE Trans. Smart Grid*, Early Access

[28] W. Deng, N. Y. Dai, K. Lao and J. M. Guerrero, "An Enhanced Power Decoupling Control for Grid-connected Capacitive-Coupling Inverters,"

ECCE 2019 - IEEE Energy Convers. Congr. Expo. Proc., pp. 1466-1473, 2019

[29] N-Y. Dai, W.-C. Zhang, M.-C. Wong, J. M. Guerrero, and C.-S. Lam, ‘‘Analysis, control and experimental verification of a single-phase capacitive-coupling grid-connected inverter,’’ *IET Power Electron.*, vol. 8, no. 5, pp. 770–782, May 2015.

[30] H. Fujita and H. Akagi, "A practical approach to harmonic compensation in power systems-series connection of passive and active filters," in *IEEE Trans. Ind. Appl.*, vol. 27, no. 6, pp. 1020-1025, Nov.-Dec. 1991.

[31] S. Bhattacharya, P. T. Cheng, and D. M. Divan, “Hybrid solutions for improving passive filter performance in high power applications,” in *IEEE Trans. Ind. Appl.*, vol. 33, pp. 732–747, May/June 1997.

[32] H. Akagi and T. Hatada, "Voltage Balancing Control for a Three-Level Diode-Clamped Converter in a Medium-Voltage Transformerless Hybrid Active Filter," in *IEEE Trans. Power Electron.*, vol. 24, no. 3, pp. 571-579, March 2009.

[33] H. Akagi and K. Isozaki, "A Hybrid Active Filter for a Three-Phase 12-Pulse Diode Rectifier Used as the Front End of a Medium-Voltage Motor Drive," in *IEEE Trans. Power Electron.*, vol. 27, no. 1, pp. 69-77, Jan. 2012.

[34] C. Lam, M. Wong and Y. Han, "Hysteresis current control of hybrid active power filters," in *IET Power Electron.*, vol. 5, no. 7, pp. 1175-1187, August 2012.

[35] T. Ye, N. Dai, C. Lam, M. Wong and J. M. Guerrero, "Analysis, Design, and Implementation of a Quasi-Proportional-Resonant Controller for a Multifunctional Capacitive-Coupling Grid-Connected Inverter," in *IEEE Trans. Ind. Appl.*, vol. 52, no. 5, pp. 4269-4280, Sept.-Oct. 2016.

[36] K. Lao, W. Deng, J. Sheng and N. Dai, "PQ-Coupling Strategy for Droop Control in Grid-Connected Capacitive-Coupled Inverter," *IEEE Access*, vol. 7, pp. 31663-31671, 2019.

[37] W. Sou et al., "A Deadbeat Current Controller of LC-Hybrid Active Power Filter for Power Quality Improvement," in *IEEE J. Emerg. Sel. Topics Power Electron.*, Early Access.

[38] C. Gong, W. Sou and C. Lam, "Second-Order Sliding Mode Current Controller for LC-Coupling Hybrid Active Power Filter," in *IEEE Trans. Ind. Electron.*, Early Access.

[39] T. Ye, N. Dai, K. W. Lao, C.-S. Lam, and M.-C. Wong, “Low DC voltage PV generation system with power factor correction and harmonic suppression capability in a distribution network,” *IET Gener. Transm. Distrib.*, vol. 13, no. 7, pp. 1049–1056, Apr. 2019.

[40] Lao, K. W., Dai, N. Y.,Sheng, J. J., “An improved closed-loop droop control technique for higher utilization of power output capability in CCI”, *Int. J. of Electri. Power & Energy Sys.*, Vol. 109, (07/2019): 455-469.

Wenyang Deng received the B.S. degree in electrical engineering and its automation from Taiyuan University of Science and Technology, Shanxi, China, in 2013, the M.Sc. degree in electrical power system engineering from University of Manchester, Manchester, U.K., in 2014. He is currently a Ph.D. candidate in University of Macau, Macao SAR, China.

His research interests include regulation of capacitive-coupling converter, hybrid converter's power sharing, and power quality improvement in microgrids.

Ningyi Dai (S'05-M'08-SM'15) received the B.Sc. degree in Electrical Engineering from Southeast University, Nanjing, China, in 2001, and the M.Sc. and Ph.D. degrees in Electrical and Electronics Engineering from the Faculty of Science and Technology, University of Macau, Macau, China, in 2004 and 2007, respectively, where she is currently an Associate Professor with the Department of Electrical and Computer Engineering.

She has authored or co-authored more than 70 technical journals and conference papers in the field of power system and power electronics. Her current research interests include application of power electronics in power systems, renewable energy integration, and integrated energy system. She was a co-recipient of the Macao Science and Technology Invention Award in 2012 and 2018 respectively.

Keng-Weng Lao (S'09–M'17) received the B.Sc., M.Sc., and Ph.D. degrees in Electrical and Electronics Engineering from the Faculty of Science and Technology, University of Macau, Macao, in 2009, 2011, and 2016, respectively. He is currently an assistant professor in the Department of Electrical and Computer Engineering and State Key Laboratory of Internet of Things for Smart City at University of Macau.

His research interests include power quality compensation, renewable energy integration, energy saving, energy internet of things, energy big data analysis and power system.

Josep M. Guerrero (Fellow, IEEE) received the B.S. degree in telecommunications engineering, the M.S. degree in electronics engineering, and the Ph.D. degree in power electronics from the Technical University of Catalonia, Barcelona, Spain, in 1997, 2000, and 2003, respectively.

Since 2011, he has been a Full Professor with the Department of Energy Technology, Aalborg University, Aalborg, Denmark, where he is responsible for the Microgrid Research Program. Since 2014, he has been the Chair Professor with Shandong University, Jinan, China. Since 2015, he has been with a Distinguished Guest Professor with Hunan University, Changsha, China. Since 2016, he was a Visiting Professor Fellow with Aston University, Birmingham, U.K., and a Guest Professor with the Nanjing University of Posts and Telecommunications, Nanjing, China. In 2019, he became a Villum Investigator by The Villum Fonden, which supports the Center for Research on Microgrids (CROM) at Aalborg University, being the Founder and the Director of the center. He has published more than 500 journal articles in the fields of microgrids and renewable energy systems, which are cited more than 50 000 times. His research interests are oriented to different microgrid aspects, including power electronics, distributed energy-storage systems, hierarchical and cooperative control, energy management systems, smart metering, and the Internet of Things for ac/dc microgrid clusters and islanded minigrids. He specially focused on microgrid technologies applied to offshore wind, maritime microgrids for electrical ships, vessels, ferries and seaports, and space microgrids applied to nanosatellites and spacecrafts.

Prof. Guerrero was elevated as an IEEE Fellow for his contributions on distributed power systems and microgrids in 2015. He received the Best Paper Award of the IEEE TRANSACTIONSON ENERGY CONVERSION for the period 2014–2015, the Best Paper Prize of the IEEE PES in 2015, and the Best Paper Award of the Journal of Power Electronics in 2016. During six consecutive years, from 2014 to 2019, he was awarded by Clarivate Analytics (former Thomson Reuters) as a Highly Cited Researcher. He is an associate editor for many IEEE TRANSACTIONS.